Title

GOLGA8 increases bulk antisense oligonucleotide uptake and activity in mammalian cells.

Authors

McMahon, Moira
Rahdar, Meghdad
Mukhopadhyay, Swagatam
et al.

Publication Date

2023-06-13

DOI

10.1016/j.omtn.2023.03.017

Peer reviewed

Molecular Therapy
Nucleic Acids
Original Article

GOLGA8 increases bulk antisense oligonucleotide uptake and activity in mammalian cells

Moira A. McMahon,[1,4] Meghdad Rahdar,[1,4] Swagatam Mukhopadhyay,[1,3] Huynh-Hoa Bui,[1] Christopher Hart,[1,3] Sagar Damle,[1] Margo Courtney,[1] Michael W. Baughn,[2] Don W. Cleveland,[2] and C. Frank Bennett[1]

[1]Ionis Pharmaceuticals, Inc., Carlsbad, CA 92010, USA; [2]Ludwig Institute for Cancer Research, University of California at San Diego, La Jolla, CA 92093-0670, USA

Antisense oligonucleotides (ASOs) are short synthetic nucleic acids that recognize and bind to complementary RNA to modulate gene expression. It is well established that single-stranded, phosphorothioate-modified ASOs enter cells independent of carrier molecules, primarily via endocytic pathways, but that only a small portion of internalized ASO is released into the cytosol and/or nucleus, rendering the majority of ASO inaccessible to the targeted RNA. Identifying pathways that can increase the available ASO pool is valuable as a research tool and therapeutically. Here, we conducted a functional genomic screen for ASO activity by engineering GFP splice reporter cells and applying genome-wide CRISPR gene activation. The screen can identify factors that enhance ASO splice modulation activity. Characterization of hit genes uncovered GOLGA8, a largely uncharacterized protein, as a novel positive regulator enhancing ASO activity by ~2-fold. Bulk ASO uptake is 2- to 5-fold higher in GOLGA8-overexpressing cells where GOLGA8 and ASOs are observed in the same intracellular compartments. We find GOLGA8 is highly localized to the *trans*-Golgi and readily detectable at the plasma membrane. Interestingly, overexpression of GOLGA8 increased activity for both splice modulation and RNase H1-dependent ASOs. Taken together, these results support a novel role for GOLGA8 in productive ASO uptake.

INTRODUCTION

Antisense oligonucleotides (ASOs) are short, chemically modified nucleic acid analogs that base pair with a target RNA, primarily making the RNA a substrate for cleavage by the enzymes RNase H1 and Ago2 or by altering pre-mRNA splicing.[1–3] Chemical modifications to ASOs include phosphorothioate (PS) backbone substitution and sugar modifications such as 2′-fluoro, 2′-methoxy, 2′-O-methoxyethyl (MOE), locked nucleic acid (LNA), and S-constrained ethyl (cEt).[4,5] RNase H1-enabling ASOs contain a DNA segment flanked on either side with chemically modified residues, whereas splice-modulating ASOs are generally chemically modified throughout the oligo.[6] Chemical modification has been demonstrated to increase metabolic stability and improve distribution into cells and tissues.[4,6] Therapeutically, PS-modified single-stranded ASOs injected subcutaneously or intravenously readily bind plasma proteins, preventing excretion into the urine and facilitating tissue distribution.[7] Importantly, ASOs are active at engaging target RNA in both the cytoplasm and nucleus.[8]

Single-stranded PS-ASOs enter cells in the absence of carrier molecules and accumulate in cells via productive and non-productive pathways.[9,10] In productive uptake, ASOs are trafficked through the endocytic pathway and are released from membrane-bound vesicles, enabling ASOs to interact with target RNAs.[9–14] In a non-productive pathway, e.g., macropinocytosis, ASOs are sequestered from their cognate target RNAs and have largely been found to localize to lysosomes. Although internalization and trafficking of ASOs can vary by cell type, it is evident that only a small fraction of internalized ASOs are released from endocytic organelles to interact with target RNA and that the majority of ASOs are trafficked through a non-productive pathway.[15] A better understanding of proteins necessary for trafficking ASOs through membrane-bound endocytic organelles and the factors facilitating release into the cytoplasm will be important for improving drug efficacy.

Pooled genome-wide screens using the Clustered Regularly Interspaced Short Palindromic Repeats (CRISPR)-associated nuclease Cas9 system have enabled a better understanding of the gene function important for various mechanisms.[16–19] Traditional CRISPR-Cas9 targeting requires co-expression of a single guide RNA (sgRNA) and Cas9 protein, which complex in an sgRNA-specific manner with target DNA to induce a double-stranded break.[20–22] Alternatively, Cas9 nuclease dead variants fused with various gene modulators can site-specifically regulate gene expression.[23] Pooled screens using tens of thousands of sgRNAs targeting protein coding genes for knockout, activation, or silencing have been useful for identifying

Received 30 November 2022; accepted 23 March 2023;
https://doi.org/10.1016/j.omtn.2023.03.017.

[3]Present address: Creyon Bio, Inc., San Diego, CA 92008, USA

[4]These authors contributed equally

Correspondence: Moira A. McMahon, Ionis Pharmaceuticals, Inc., 2855 Gazelle Court, Carlsbad, CA 92010, USA.
E-mail: mmcmahon@ionisph.com

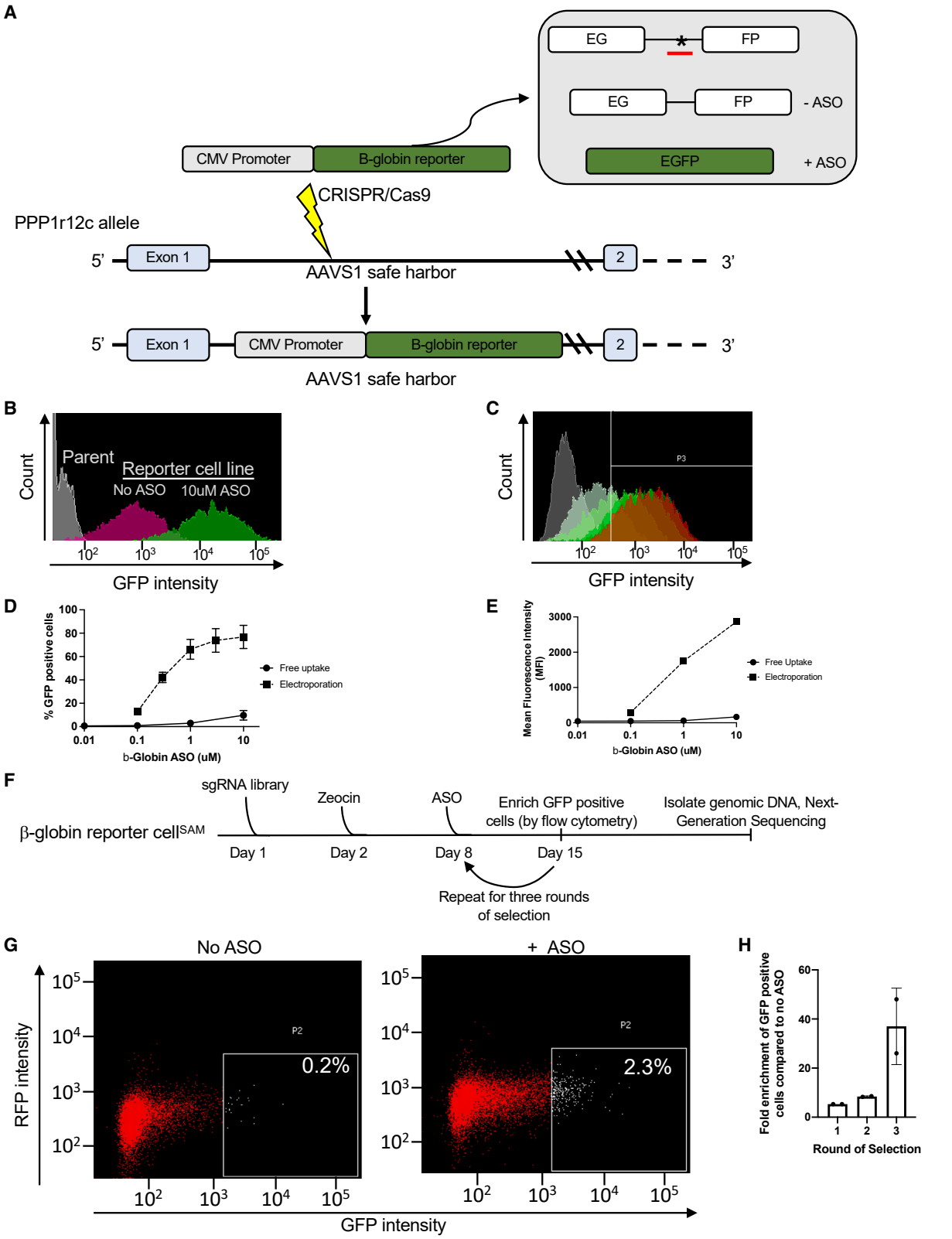

(legend on next page)

key proteins important in various cell mechanisms.[16–19] Application of a CRISPR-Cas9-based screen would be valuable for elucidating pathways and proteins mediating productive ASO uptake.

Here, we present a pooled CRISPR-Cas9 gene activation strategy in an ASO-sensitive splice reporter engineered cell line for identifying genes important for mediating productive uptake of ASOs. Previous studies have addressed this question using cell lines that demonstrate efficient productive ASO uptake that, upon gene silencing, lose this ability.[24] In this study, we used cells that demonstrate poor productive uptake and used a gene activation strategy to identify genes that enable cells to become more efficient for productive ASO uptake. We transduced engineered K562 cells expressing an ASO-sensitive green fluorescent protein (GFP) reporter with a pooled, genome-wide library of sgRNA-expressing lentiviruses and treated with ASO for 1 week, followed by flow cytometry to isolate GFP expressing cells (more than three rounds of selection). We recovered several genes of interest and identified the highly uncharacterized *GOLGA8* gene family as an important gene in modulating productive ASO uptake.

RESULTS

Generation of β-globin ASO reporter cell line

We generated an ASO splice reporter K562 cell line, demonstrated to be poor at productive ASO uptake (Figure S1A), to measure ASO activity in a reproducible and high-throughput manner (Figure 1A). In this approach, a gene expression cassette containing the coding sequence for GFP is separated by point mutant (C-to-T mutation at nucleotide 654) human β-globin intron-2, activating an aberrant 5′ and 3′ splice site rendering an mRNA incapable of GFP expression.[25] Upon addition of an ASO targeting the aberrant splice site, proper splicing is restored and functional GFP translated (Figure 1A). Genetically engineered K562 cells expressing the ASO-sensitive GFP reporter cassette were generated by CRISPR-Cas9 gene editing to the *AAVS1* safe harbor locus. Correct integration of the reporter was confirmed by PCR (Figure S1B) and Sanger sequence analysis (data not shown). ASO sensitivity of the K562 GFP reporter clonal cell line was tested by electroporation (Figures 1B–1E) or addition of ASO to the culture medium (Figures 1D and 1E). GFP expression is ∼20-fold higher in cells electroporated with 10 μM ASO compared with cells without ASO and over 100-fold higher compared with the parental K562 cell line in the absence of ASO (background fluorescence) (Figure 1B). Increases in GFP expression are dose dependent, as increasing amounts of electroporated ASO led to increased number of cells expressing GFP and increased GFP intensity, reaching saturation at ∼1 μM ASO (Figures 1C and 1D). By contrast, addition of 10 μM ASO to the culture medium resulted in a lower percentage of cells expressing GFP (∼12% positive compared with 80% by equivalent electroporation) (Figure 1D), and lower GFP intensity (∼20-fold) compared with cells electroporated with the same amount of ASO (Figure 1E), demonstrating that K562 cells are naturally poor at productive ASO uptake.

A genome-wide pooled sgRNA library screen in ASO reporter cell line

We performed two independent, pooled genome-wide screens using a lentiviral library containing 70,290 guide RNAs (gRNAs) targeting 23,430 genes. For each replicate, ∼200 million cells were infected with the library at a multiplicity of infection (MOI) of 0.2 to reduce the chance of more than one gRNA being expressed in each cell, incubated for 7 days with zeocin to select for transduced cells, followed by addition of ASO to the culture medium. Following 1 week in the presence of ASO, GFP-positive cells were sorted using fluorescence-activated cell sorting (FACS) and the ASO incubation repeated for a total of three rounds of selection before amplification and sequencing of gRNAs from the GFP-enriched cells (Figure 1F). ASO-incubated cells with GFP intensity greater than 10-fold above background (∼2.3% of cells) were sorted and re-cultured continuously with ASO (Figure 1G, representative plot). As shown in Figure 1H, each round of cell sorting resulted in enrichment of GFP-positive cells (∼30-fold by the third round) and was dependent on the presence of ASO, such that, when ASO was removed from the enriched GFP-positive cells, cells were no longer green (Figure S1C).

We established a computational method to address the inherent noise associated with pooled screens to identify top-ranking genes. We define the population density of each guide at each round of selection as the ratio of read counts (parts per million [PPM]) to the count in the starting pool. We can estimate the survival probability $P(s, t)$, which is a direct measure of fitness in this artifical selection setting, or, equivalently, the importance of the guide for the phenotype (see section "materials and methods"). Therefore, the density, as defined, is a direct measure of survival probability or fitness.

With few rounds of selection implemented here, it suffices to study the principal components of the population density $\rho(s, t)$. We observe that the major trend is indeed positive selection, with population representation increasing with rounds (Figure 2A, blue line).

Figure 1. Generation of ASO activity reporter cell line and genome-scale gene activation screening

(A) CRISPR-Cas9-mediated integration of eGFP reporter in the first intron of the *PPP1r12c* gene. Reporter contains an aberrant splice site in intronic sequence that, in the presence of ASO (red), is blocked such that the cells can express eGFP and in the absence of ASO do not have color. (B) FACS plot depicting the GFP intensity on the x axis versus cell count on the y axis for the reporter cell line. Reporter cells cultured in the presence of ASO (green) or absence of ASO (purple). (C) GFP intensity of reporter cell lines cultured in the presence of increasing amounts of ASO (lowest ASO concentration in light green and highest in red). (D) Percentage GFP-positive cells in the presence of increasing ASO by free uptake (circle, solid line) or electroporation (square, dotted line). (E) Mean fluorescence intensity (MFI) of cells in the presence of increasing ASO by free uptake (circle, solid line) or electroporation (square, dotted line). (F) Experimental timeline for three rounds of selection in the presence of ASO. (G) FACS plot showing the percentage and intensity of GFP-positive cells in the absence (left) and presence (right) of ASO. (H) Fold enrichment of GFP-positive cells in the presence of ASO over the three rounds of selection (GFP-positive sorting). (D, E, and H) Each experiment was done in duplicate, and error bars represent standard error of the mean.

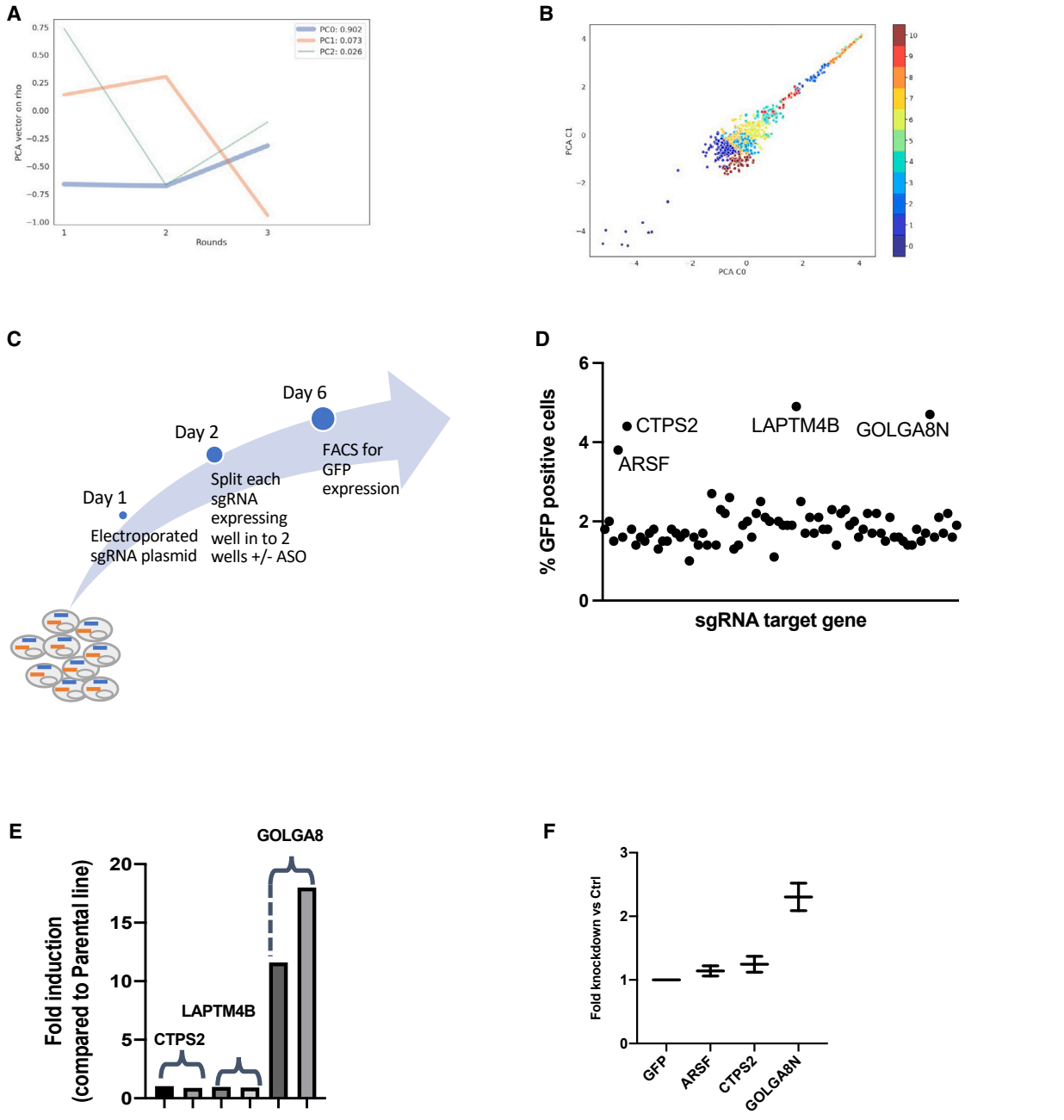

Figure 2. Genome-scale gene activation screen identifies genes that mediate productive ASO uptake

(A) Representative principal-component analysis for each round of selection (from one representative replicate) and with non-zero representation in preselection and first two rounds of ASO treatment selection. Thickness of line depicts number of guides represented. (B) Correlation of PCA component of interest (growth trend) between two biological replicates. (C) Experimental timeline for electroporating sgRNA expression plasmid into cells to confirm sgRNA hits identified in primary screening. (D) Percentage of GFP-positive cells following transient expression of individual sgRNA targeting genes identified in primary screen on the x axis following experimental design described in (C). ARSF, CTPS2, LAPTM4B, and GOLGA8N were distinct from all other guides in replicate experiments with a p value <0.0001 as shown in Figure S3A. (E) Fold induction of target genes, as measured by quantitative real-time PCR, following transient expression of individual sgRNA targeting genes indicated above bars. Each bar represents a unique primer probe set for the target gene indicated above the bars (sequence in section "materials and methods"). Each experiment was done in duplicate. (F) Fold knockdown of *MALAT1* RNA following transient transfection with CRISPR-Cas9 gene activation plasmids and indicated sgRNA expression plasmid. The 100 nM *MALAT1* ASO was added 24 h following transfection of plasmids, and knockdown analysis was done after an additional 24 h. Each experiment was done in duplicate, and error bars represent standard error of the mean.

The second most common trend is elimination from the population, and the third is stochastic behavior (see Figure 2A, brown and green lines respectively). We observed good agreement between the principal-component analysis (PCA) component of interest (the growth trend) between the two biological replicates, especially for highly fit guides (Figure 2B). This suggests that selection is robust. From the computational analysis, we generated a list of 76 top gRNAs as positive regulators of productive ASO uptake (Figure S2).

Positive regulators of productive ASO uptake validated using individually cloned gRNA expression plasmids

We individually cloned each of the top gRNAs into an expression vector and introduced them by electroporation into the reporter cell line to confirm the ability to enhance productive ASO uptake (Figure 2C). The percentages of GFP-positive cells with expression of individual gRNAs in the presence of ASO as part of a secondary screen to confirm top hits are shown in Figure 2D. Expression of gRNAs to *ARSF*, *CTPS2*, *LAPTM4B*, and *GOLGA8N* genes reproducibly demonstrated >2-fold enhancement in the number of GFP-positive cells in the presence of ASO compared with cells expressing gRNAs to other genes (Figures 2D and S3A). Interestingly, in concordance with the primary screen, the GOLGA8N guide increased in population density by almost 50-fold in both biological replicates by round 3 compared with round 1 (ARSF by 35-fold, CTPS2 by 60-fold, and LATPM4B by roughly 50-fold).

We isolated RNA from cells on day 6 (Figure 2C) and determined RNA expression of *ARSF*, *CTPS2*, *LAPTM4B*, or *GOLGA8N* using quantitative real-time PCR. *GOLGA8N* RNA was induced (>10-fold) by its gRNA as shown in Figure 2E. This was also confirmed by digital gene expression (DGE) analysis (Figures S3B and S3C). *ARSF* could not be amplified with multiple primer/probe sets, and CRISPOR analysis[26] revealed a highly repetitive sequence at the gRNA binding site resulting in greater than 700,000 potential off-target binding loci (each containing fewer than four mismatches). Similarly, a further increase in *CTPS2* or *LAPTM4B* RNA upon expression of their respective gRNAs was not observed using two different primer/probe sets (Figure 2E). Previously published work has shown that activation of gene expression using CRISPR systems is most robust for genes that exhibit low basal expression levels,[19] and quantitative RT-PCR showed *CTPS2* and *LAPTM4B* expression in K562 cells comparable with the housekeeping gene *GAPDH* (Figure S4A). It is possible that these gRNAs could be engaging additional gene targets as CRISPOR analysis predicts both also bind in highly repetitive regions[26] (Figure S4B).

We next tested whether individual expression of the gRNAs could also enhance activity of RNase H1-dependent ASOs. HEK293FT cells were transiently transfected with the CRISPR activation system plasmids and individual gRNA-expressing plasmids and incubated with 100 nM *MALAT1*-targeting ASO starting 24 h after plasmid transfection. Forty-eight hours after ASO addition, cells were harvested and RNA isolated for quantitative PCR analysis. The GOLGA8N gRNA-expressing cells demonstrated the most robust enhancement of *MALAT1* knockdown (Figure 2F), similar to the 1.5- to 2-fold improvement in activity seen in our splice reporter assay, while ARSF and CTPS2 failed to increase activity of the *MALAT1* ASO. Therefore, we chose to focus on the highly uncharacterized GOLGA8N protein.

GOLGA8N is a member of a core duplicon gene family

GOLGA, or golgin genes, encode coiled-coil proteins that are localized to the Golgi apparatus and are predicted to adopt an extended conformation into the cytoplasm, enabling tethering of membranes.[27] This membrane tethering is important for both the structural integrity of the Golgi apparatus and vesicle trafficking, but a complete understanding of golgin function has yet to be established. Interestingly, there is limited literature describing GOLGA8N, which has ~36% homology to GOLGA2 (GM130), a *cis*-Golgi protein that has been shown to help maintain structure of the Golgi apparatus and act as a tether facilitating vesicle fusion to the Golgi membrane.[28,29] Upon further bioinformatic analysis of the GOLGA8N gRNA sequence (Figure S5A), we identified four additional perfectly matched binding sites in *GOLGA8M*, *GOLGA8O*, *GOGLA8Q*, and *GOLGA8R*. Sequence alignment (Figure S5B) of these GOLGA8 proteins revealed that they are nearly identical (>99% homology) even at the RNA level. Indeed, it has previously been reported that *GOLGA8* has human-specific core duplicons that are expanded along chromosome 15q13.3[30] and are located in a highly unstable region. The *GOLGA8* subfamily includes 15 duplicated copies in this chromosomal region (Figure S5C). We herein use GOLGA8N interchangeably with GOLGA8 to include highly homologous family members.

The most similar GOLGA8 protein in mouse is GOLGA2, which shares less than 35% sequence homology. We tested whether human GOLGA8 cDNA expression in a mouse cell line could affect productive ASO uptake activity. To do this, we electroporated a human GOLGA8 cDNA expression plasmid into a mouse cell line, Hepa1-6 (which normally exhibits poor productive ASO uptake) and observed ~3-fold improvement in ASO activity compared with cells expressing a control mCherry expression plasmid (Figures S6A and S6B).

GOLGA8 localizes to both the *trans*-Golgi and inner plasma membrane

To further characterize GOLGA8 protein, we performed immunofluorescence staining in HeLa and HEK293FT cells. As shown in Figure 3A, HeLa cells transfected with a plasmid encoding a GOLGA8-mCherry fusion construct showed complete overlap in localization between the GOLGA8-specific antibody (Figures S7A and S7B) and mCherry fluorescence. Interestingly, GOLGA8 appeared to localize to an intensely fluorescent perinuclear structure, indicative of the Golgi apparatus, as well as strong plasma membrane staining.

We wanted to test whether GOLGA8 localized on the inner or outer leaflet of the plasma membrane. To do this, HEK293FT cells were transfected with a GOLGA8 expression construct and, 24 h following transfection, fixed with 4% paraformaldehyde or fixed and permeabilized with Triton X-100 prior to staining with the GOLGA8 primary

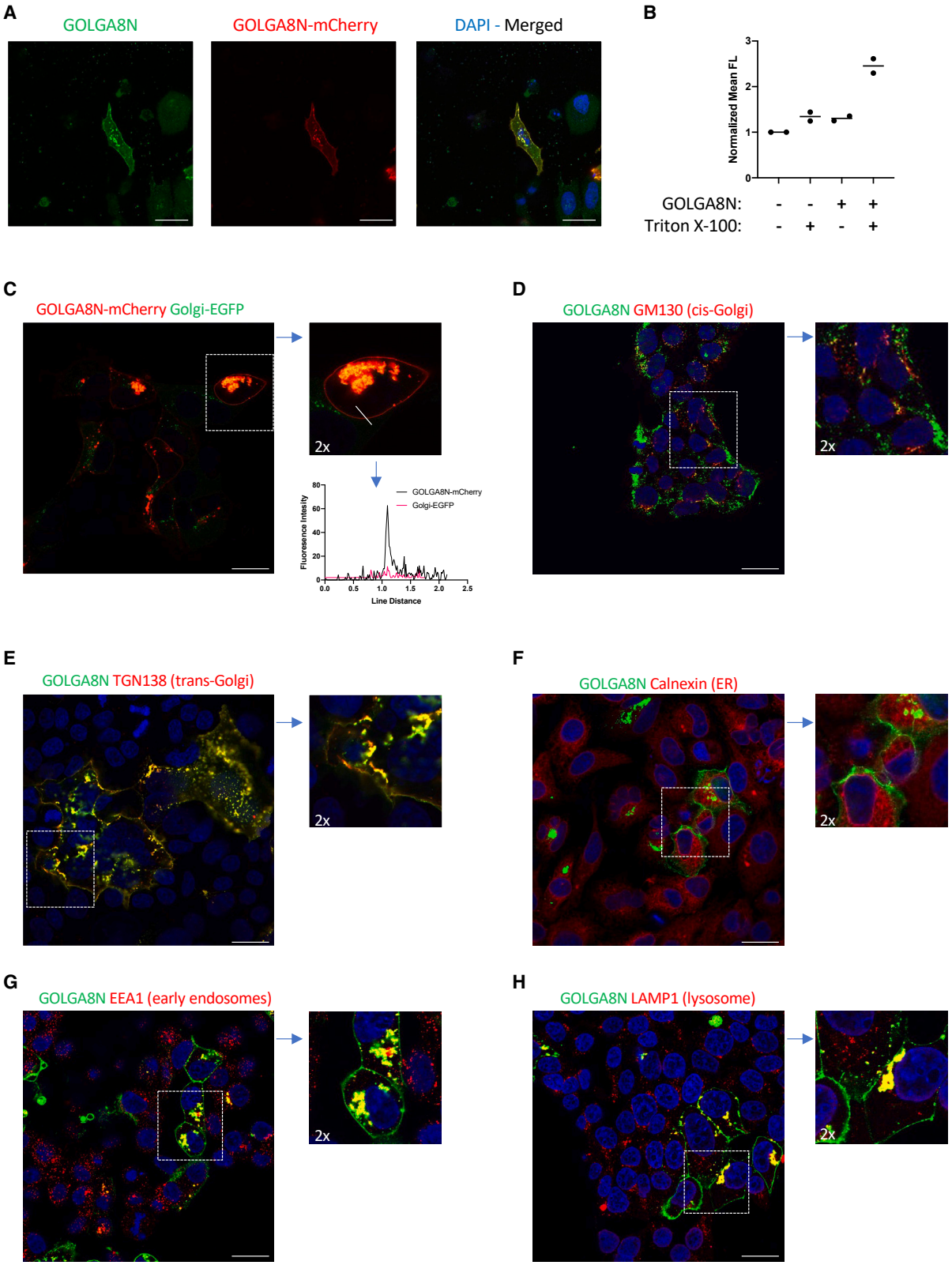

(legend on next page)

antibody and Alexa 488 rabbit secondary antibody. As shown in Figure 3B, GOLGA8 was only detected in cells treated with Triton X-100 where the mean fluorescence was ~3-fold above background, suggesting that GOLGA8 is on the inner plasma membrane and only accessible to the antibody when the cells are permeabilized.

Next, we wanted to confirm that the perinuclear staining seen in Figure 3A was in fact Golgi and to determine whether GOLGA8 could be found in any other cellular compartments. We co-expressed GOLGA8-mCherry with a commercially available Golgi-eGFP expression cassette. GOLGA8-mCherry and Golgi-eGFP demonstrate strong co-localization (Figure 3C). We observed GOLGA8-mCherry highly localized along the plasma membrane where Golgi-eGFP is completely absent.

We observed very little co-staining of GOLGA8 with the *cis*-Golgi marker GM130 (Figure 3D) compared with the highly correlated co-staining of GOLGA8 with the *trans*-Golgi marker TGN138 (Figure 3E). To detect a more robust GOLGA8 signal, we expressed a GOLGA8-HA expression construct in HeLa cells for co-staining with additional intracellular compartment markers. At steady state, very little GOLGA8 was observed in the endoplasmic reticulum (ER) (Figure 3F). Some GOLGA8 was also observed in early endosomes and lysosomes (Figures 3G and 3H respectively). Together, these results suggest that GOLGA8 is mainly a *trans*-Golgi- and plasma-membrane-localized protein.

GOLGA8 increases bulk ASO uptake in cells that are poor at productive ASO uptake

We observed that both CRISPR activation-induced expression of endogenous GOLGA8 and transfection of a GOLGA8 cDNA expression construct resulted in ~2-fold improvement in activity of both splicing- and RNaseH1 degradation-mediated ASOs. To better understand how GOLGA8 mediates this improved activity, we tested whether GOLGA8 expression could similarly change the bulk uptake of ASOs into cells. To do this, HEK293FT cells were transfected with GOLGA8 cDNA expression plasmid and cultured for 24 h. Next, CY3-MALAT1 ASO was added to the culture medium at a final concentration of 100 nM and incubated for an additional 24 h before cells were analyzed by flow cytometry. As shown in Figure 4A, the Cy3 mean fluorescence intensity of cells expressing GOLGA8 is about five times higher than control cells transfected with a GFP plasmid, suggesting that GOLGA8 expression results in an increase in bulk ASO uptake.

We next wanted to determine whether this increase in bulk ASO uptake is concentration dependent. To do this, we performed the experiment as in Figure 4A but added ASO at final concentrations ranging from 3 to 3,000 nM. The experiment was performed multiple times (more than five separate replicates) and, as shown by Figure 4B, CY3-MALAT1 ASO mean fluorescence in GOLGA8 expressing cells was ~2-fold higher at all ASO concentrations tested. In addition, a similarly performed experiment using fluorescently labeled dextran, which enters cells through micropinocytosis, or transferrin, which enters cells through receptor-mediated endocytosis (Figures 4C and 4D, respectively), showed no difference in mean fluorescence intensity in untreated control cells compared with GOLGA8-overexpressing cells. This suggests that the increased bulk uptake in GOLGA8-expressing cells is ASO specific. Importantly, using live-cell confocal imaging, GOLGA8-mCherry and MALAT1-A488 ASO can be seen in overlapping or adjacent puncta, while this is not the case for other genes tested from the screen (Figures 4G and S9).

We next wanted to test whether GOLGA8 overexpression in cells already efficient at productive uptake could further improve ASO activity. To do this, we used A431 epidermoid carcinoma cells, a naturally efficient productive uptake line. As shown in the dose-response curve in Figure 4E, the half maximal inhibitory concentration (IC_{50}) for knockdown of the MALAT1 long non-coding RNA (lncRNA) with MALAT1 ASO in A431 cells is 50-fold lower than in HEK293FT (~6 nM vs. 300 nM). We co-transfected a GFP expression construct (to identify transfected cells) and GOLGA8 expression construct followed by ASO incubation. All cells took up ASO, and further analysis of cells that were transfected (Figure S8) did not show a difference in the amount of ASO bulk uptake (Figure 4F). Several attempts to knock down GOLGA8 expression using small interfering RNA (siRNA) were unsuccessful due to low transfection efficiency and difficulty quantifying GOLGA8 endogenous protein levels by western blot (data not shown).

DISCUSSION

CRISPR-Cas9 pooled genetic screens have become a useful tool for interrogating key players in a variety of cellular phenotypes. Many examples demonstrating the utility of this approach[16–19] have fueled the excitement to continue to use the technology to address long-standing unanswered questions. Here, we used a CRISPR-Cas screen to identify novel genes that are important for facilitating productive ASO uptake.

Figure 3. GOLGA8 localizes to Golgi apparatus and plasma membrane

(A) HeLa cells were transiently transfected with GOLGA8-mCherry expression plasmid. Representative images of localization of GOLGA8 using a GOLGA8-specific antibody (left) or mCherry fluorescence (right). Magnification bar represents 30 μm. (B) Localization of GOLGA8 at the inner plasma membrane by flow cytometry analysis following fixation, permeabilization, and antibody staining. Experiment was done in duplicate and error bars represent standard error of the mean. (C) Localization of GOLGA8-mCherry in Golgi-eGFP-expressing cells (left image) and 2× magnification (dotted white box, and right image). Fluorescence intensity was measured over indicated line in right image and plotted over distance (bottom graph). (D–H) HeLa cells were transiently transfected with GOLGA8 expression plasmid followed by fixation and stained .for GOLGA8 (green) and (D) cis-Golgi marker, GM130, (E) trans-Golgi marker, TGN138, (F) endoplasmic reticulum (ER) marker, calnexin, (G) early endosome marker, Early Endosome Antigen 1 (EEA1) and (H) lysosome marker, lysosomal-associated membrane protein-1 (LAMP1), in red. Nuclei were stained with DAPI (blue). Magnification bar represents 25 μm.

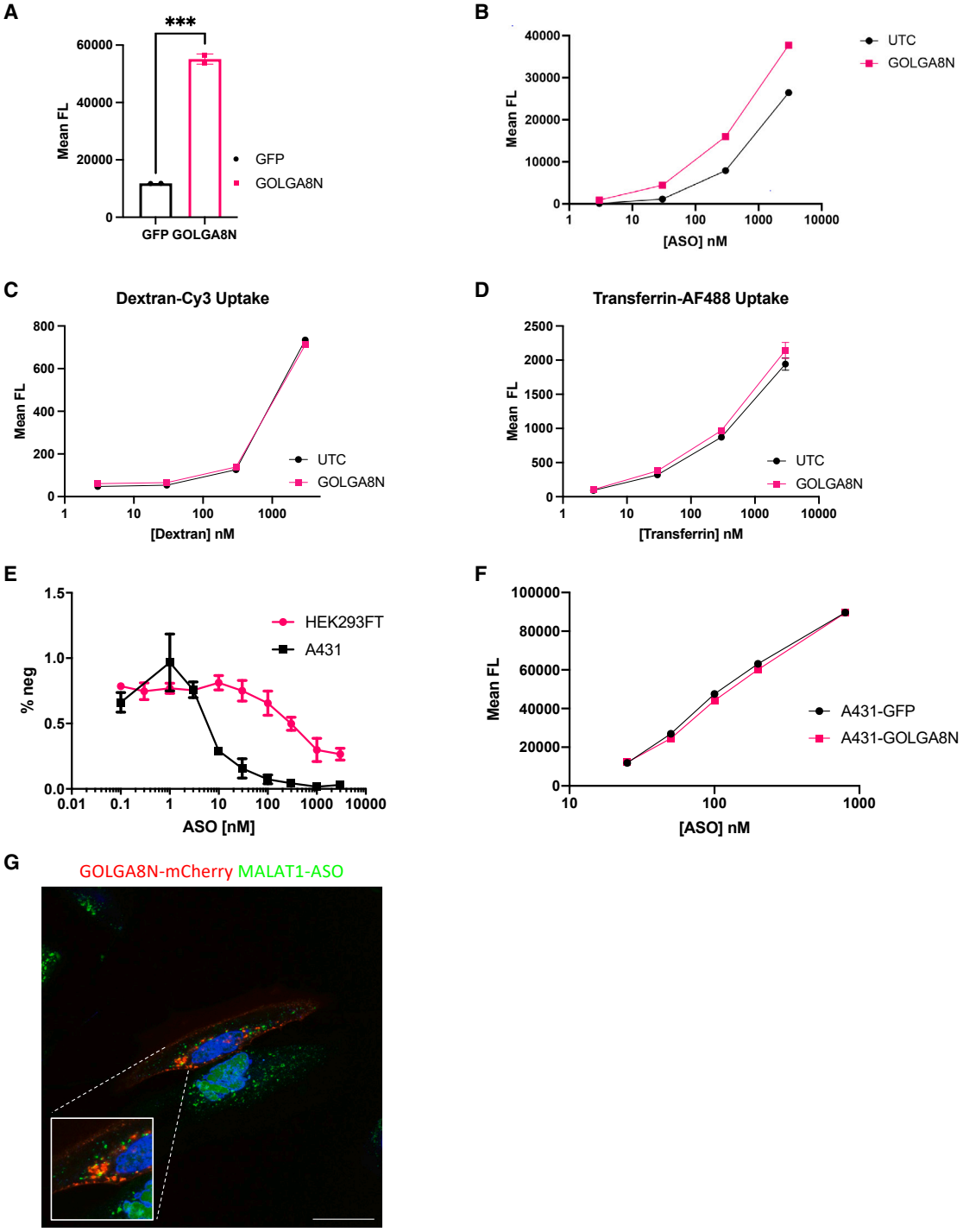

Figure 4. GOLGA8 overexpression enhances bulk ASO uptake in HEK293FT cells

(A) HEK293FT cells transfected with GOLGA8-HA epitope tagged expression plasmid (red bar) and 24 h later incubated with 100 nM Cy3-MALAT1-ASO. Mean fluorescence of cells (y axis) was measured by flow cytometry 24 h after ASO addition compared with cells expressing GFP alone (black bar). ***$p < 0.0008$. Each condition was done in duplicate and standard error of mean to determine variation. (B) HEK293FT cells transfected with either GOLGA8-HA expression plasmid (red line, square) or Lipofectamine control (black line, circle, untreated control [UTC]) were subjected to increasing amounts of Cy3-MALAT1-ASO and mean fluorescence analyzed by flow cytometry. The experiment was performed in triplicate. (C) Same experimental design as in (B) except addition of Dextran-Cy3 instead of ASO in duplicate. (D) Same experimental design as in (B) except addition of AlexaFluor488-Transferrin for 7 h before FACS analysis in duplicates. (E) Comparative MALAT1 ASO dose-response curves by addition of ASO to

(legend continued on next page)

It is well established that the productive ASO pathway proceeds via endocytosis. Upon entering cells, ASOs are trafficked through early endosomes (EEs) within 10–20 min, late endosomes (LEs) within 20–60 min, and ultimately lysosomes within about an hour.[31] ASO activity is observed several hours after free uptake (>6 h), suggesting a slow release of ASO from endocytic organelles.[12] Several mechanisms have been proposed for escape of ASOs from LEs or multivesicular bodies.[9,12,32] A recently published finding demonstrated that the *trans*-Golgi network (TGN)-LE transport pathway facilitates ASO release from the endocytic pathway.[33] The mannose-6-phosphate receptor (M6PR), which binds to M6P-tagged hydrolases, traffics from the *trans*-Golgi to LEs and finally to lysosomes. M6PR-containing vesicles are recycled back to the TGN[34] and fuse to TGN membranes through interaction with GCC2, a TGN peripheral membrane vesicle-tethering protein.[35,36] ASOs strongly co-localize with M6PR and GCC2, and reduction of these proteins using siRNAs decreased ASO activity.[33] The data support a role for vesicles that transport through the Golgi apparatus in facilitating ASO release. Intriguingly here, using an unbiased genome-wide screening approach, we identified another *trans*-Golgi localized tethering protein, GOLGA8, as a novel player mediating ASO activity.

Although the *GOLGA* genes are known to encode long coiled-coil proteins that act as tethers in the Golgi apparatus, *GOLGA8* itself is not well studied. *GOLGA8* has human-specific core duplicons with at least 15 duplicated copies, and the duplication architecture is not well defined,[30] making it a challenging gene to study. We used a GOLGA8 cDNA expression construct or GOLGA8-mCherry fusion for the majority of our ASO studies as this allowed us to visualize GOLGA8 in cells that had very low levels of endogenous GOLGA8 expression. It also confirmed that the enhancement of ASO activity was in fact GOLGA8 specific and not a potential off-target binding of the sgRNA in another gene. Interestingly, induced GOLGA8 expression in cells poor at productive ASO uptake resulted in up to 5-fold increase in bulk uptake (Figure 4A) and greater than 229 gene changes related to Golgi apparatus, cytoplasmic vesicles, and related membranes (Figures S3B–S3D). Importantly, GOLGA8 and ASO were observed in similar punctate patterns in cells (Figure 4G). Taken together, the data suggest that GOLGA8 could be important for ASO escape from endosomal organelles and that it could play a similar role to GCC2.

Based on our findings that GOLGA8 expression in cells normally poor at productive uptake resulted in an increase in ASO bulk uptake and an upregulation of genes associated with Golgi apparatus and membrane/vesicles, we developed a model for ASO movement inside GOLGA8-expressing cells. As shown in Figure 5, we propose a model where GOLGA8 could play a role at various stages of ASO-containing vesicle movement in a cell. First, as GOLGA8 is found at the plasma membrane, it could be decorating the outside of ASO-containing endocytic vesicles and bias fusion of EEs to the *trans*-Golgi since GOLGA8 is a heavily *trans*-Golgi-localized protein and likely recycled back there. The fusion of EEs with *trans*-Golgi could allow a release of ASO that can increase its chances to interact with cognate RNA in the cytoplasm or nucleus. Second, GOLGA8 at the *trans*-Golgi could be tethering ASO-containing vesicles, increasing their half-life in cells and allowing for the release of ASOs from vesicles. Third, GOLGA8 at the plasma membrane could be interacting with ASO-positive vesicles and slowing their export out of the cell, further increasing the time the vesicles are in cells and allowing more time for ASOs to be released and find their target RNA. Finally, GOLGA8, with other gene expression changes observed in this study, could be promoting retrograde trafficking of vesicles from the Golgi to the ER giving ASO more direct access to the nucleus and target RNA. Any or all of these, and possibly more scenarios, could be how GOLGA8 is increasing ASO bulk uptake/activity, but further studies are needed to fully define GOLGA8's role both in the cellular context and related to ASO activity.

In this study, we used a genome-wide CRISPR gene activation screen to identify genes that regulate productive ASO uptake. Although all cells take up ASOs, only a small proportion of ASOs, even in cells good at productive uptake, are released from intracellular organelles to interact with target RNA. We have shown that increased GOLGA8 expression in cells poor at productive uptake can influence ASO activity in a positive manner. Our study suggests a novel role for GOLGA8 in increasing ASO bulk uptake, resulting in enhanced ASO activity (2-fold) and is in agreement with other studies showing that the Golgi apparatus is an important organelle facilitating ASO activity. Extending our analysis, we looked at RNA expression levels of *GOLGA8* family members in an additional seven cell lines, a mix of good and poor productive ASO uptake cells, and did not see a correlation with GOLGA8 expression levels (data not shown). We hypothesize that a combination of GOLGA8 expression along with changes in expression of yet-to-be-identified gene/s will further enhance ASO activity beyond the 2-fold we observed here and that GOLGA8 is not sufficient or the only driver to enhance ASO activity. A better understanding of how ASOs reach their target RNA and the proteins involved in their movement in the cell will be important for future ASO drug development.

MATERIALS AND METHODS

Plasmid production

The plasmids used in this study were designed and constructed using standard molecular biology techniques, including restriction enzyme digestion, ligation, PCR, and Gibson assembly (New England Biolabs, Ipswich, MA). All oligonucleotides were purchased from Integrated DNA Technologies. Human CRISPR-3 plasmid activation pooled library (SAM) was a gift from Feng Zhang (Addgene # 1000000057).

culture medium in poor productive uptake cell line (HEK293FT, red line, circle) and good productive uptake cell line (A431, black line, square) performed in triplicate. The y axis (% neg) is the percentage of RNA compared with cells not treated with ASO. (F) Experiment design as in (B) but in A431 cell line. Each curve represents a duplicate experiment. (G) Live-cell confocal imaging of HeLa cells expressing GOLGA8-mCherry. Cells were treated with 200 nM MALAT1-ASO-A488 for 24 h. Magnification bar, 20 μm.

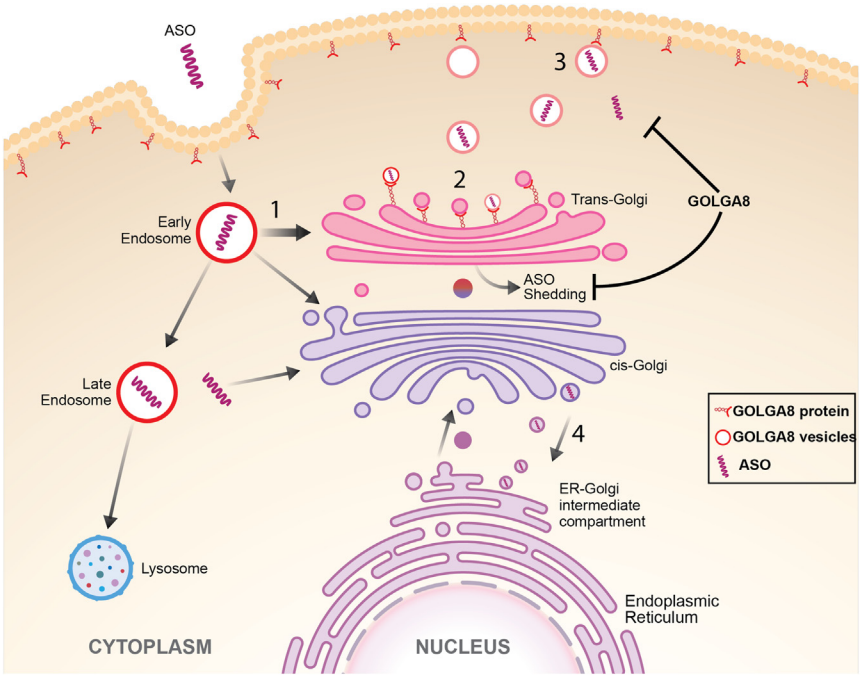

Figure 5. A model for GOLGA8 role in enhancing productive ASO uptake

GOLGA8 localized at the plasma membrane shuttling GOLGA8-positive early endosomes containing ASO mainly to the *trans*-Golgi (1), and to a lesser extent the *cis*-Golgi, and preventing their degradation in the lysosome. ASO-positive intracellular vesicles fusing with Golgi membrane could allow shedding of ASO. In addition, GOLGA8 expressed in the *trans*-Golgi may act as a tether to capture ASO-containing vesicles (2), further allowing time for ASO release before being shuttled back to the plasma membrane. Alternatively, GOLGA8 expressed at the plasma membrane could tether ASO vesicles (3) and slow their export from the cell, allowing time for ASO to shed or be released. Finally, GOLGA8 expression and subsequent Golgi, ER membrane changes may enhance the ability of retrograde trafficking of ASO-containing vesicles from the *cis*-Golgi to ER/nucleus (4).

Cell lines and transfection

K562

K562 cells (ATCC) were grown in Iscove's modified Dulbecco's medium (Life Technologies, Carlsbad, CA) supplemented with 10% fetal bovine serum (Omega Scientific, Tarzana, CA) and antibiotic-antimycotic (10,000 units/mL of penicillin, 10,000 μg/mL of streptomycin, and 25 μg/mL Fungizone). Plasmids (1 μg total for 1×10^6 cells) were electroporated into cells using the Amaxa Nucleofector 2b device and program T-016.

HEK293FT and HeLa

HEK293FT and HeLa cells (ATCC) were cultured in DMEM (Life Technologies, Carlsbad, CA) supplemented with 10% fetal bovine serum (Omega Scientific, Tarzana, CA), 25 mM HEPES, and antibiotic-antimycotic (10,000 units/mL of penicillin, 10,000 μg/mL of streptomycin, and 25 μg/mL Fungizone). Cells were transfected in six-well plates at 40% confluency using 2 μg of plasmid and Lipofectamine 3000 (Life Technologies, Carlsbad, CA).

Hepa1-6

Hepa1-6 cells (ATCC) were cultured in DMEM (Life Technologies, Carlsbad, CA) supplemented with 10% fetal bovine serum (Omega Scientific, Tarzana, CA), and antibiotic-antimycotic (10,000 units/mL of penicillin, 10,000 μg/mL of streptomycin, and 25 μg/mL Fungizone). Plasmids (1 μg total for 1×10^6 cells) were electroporated into cells using the Amaxa Nucleofector 2b device and program T-020.

Generation of reporter cells

The β-globin GFP reporter was integrated into the *AAVS1* safe harbor locus in K562 cells using CRISPR-Cas9 gene editing. An sgRNA targeting *AAVS1* was cloned into an expression plasmid (250 ng) and co-electroporated with a targeting vector (1 μg) containing the reporter sequence cloned between ~1 kb *AAVS1* left and right homology arms centered around the CRISPR-Cas9 cut site. At 48 h following electroporation, cells were single-cell sorted into 96-well plates using the FACS ARIA II. Individual clones were expanded, and DNA was extracted for PCR amplification and sequencing to confirm reporter integration at the *AAVS1* locus.

Antisense oligonucleotide treatment

For free uptake, ASOs (β-globin sequence 5′ GCTATTACCTT AACCCAG, *MALAT1* sequence 5′ CCAGGCTGGTTATGACT CAG) were directly added to the medium at different final concentrations, and cells were cultured for an additional time (as indicated in the text for individual experiments) before collection. For transfection, K562 cells were electroporated with ASOs using the same protocol as for plasmid electroporation.

Virus production and transduction

HEK293FT cells were cultured as above and virus production was as reported previously.[37] Briefly, cells were seeded at 40% confluency in T225 flasks and transfected the next day at ~80%–90% confluency using 10 μg of plasmid of interest, 10 μg of pMD2.g, and 15 μg of psPAX2 (Addgene) using Lipofectamine 2000. Four to 6 h after transfection, medium was replaced. Virus supernatant was harvested 48 h after transfection, filtered using a 0.45-μm polyvinylidene fluoride (PVDF) filter (MilliporeSigma, Burlington, MA), and stored at −80°C in 1-mL aliquots. For transduction, 500,000 cells were plated into each well of a 24-well plate with 1 mL of medium containing virus at an MOI of 0.2, and 8 μg/mL polybrene final concentration. Plates were spun for 2 h at 1000 × *g*, and cells were washed and plated on appropriate tissue culture dishes. Drug was added the day after transduction.

ASO activity screen

β-Globin reporter K562 cells stably integrated with Synergistic Activation Mediator (SAM) Cas9 and effector components were transduced with SAM sgRNA libraries at an MOI of 0.2 (guide representation of 500 transduced cells per guide) as described above. On day two post transduction, zeocin was added to culture medium and, 8 days post infection, cells were split into vehicle and β-globin ASO conditions (100 nM ASO final). Every 7 days (for three rounds), 30,000 GFP-positive cells were sorted using the FACS ARIA II and cultured for 7 days with or without ASO before harvesting cells for gDNA extraction. Genomic DNA extraction, PCR of virally integrated guides, and PCR purification of libraries were performed as previously published.[37]

NGS and screen hits analysis

NGS data were de-multiplexed using unique index reads. Guide counts were determined based on sequencing reads that matched perfectly to their respective barcode sequence. The read counts were denoted (PPM) as $n(s,t)$ for guide s at round t, where $t = 0$ is the starting pool. The population density was denoted as $\rho(s,t)$ for guide s and round t, so $\rho(s,t) = \frac{n(s,t)}{n(s,t=0)}$ Also, the survival probability of guide s not being eliminated in going from round t to $t+1$ was denoted as $P(s,t)$. Therefore, by definition, the ratio $\frac{n(s,t+1)}{n(s,t)} = \frac{P(s,t)}{\Sigma_s P(s,t)\ n(s,t)}$. Under constant survival probability, $P(s)$, it can be shown that $log[\rho(s,t)] = t\ log[P(s)] - log[\Sigma_s P(s)\ n(s,t=0)]$.

Immunoblotting

Total protein extracts were collected by scraping cells in 1× Laemmli sample buffer and boiling for 5 min, and centrifugation at 15,000×g for 5 min. Proteins were transferred to PVDF and blocked in 5% milk solution in Tris-buffered saline and 0.1% Tween 20 (TBST) for 1 h before overnight incubation with the following primary antibodies: immunoblots were washed in TBST and probed with horseradish peroxidase (HRP)-conjugated secondary antibodies diluted 1:3,000 for 1 h at room temperature (GE Healthcare, Chicago, IL) before being imaged using Bio-Rad ChemiDoc MP Imager.

GOLGA8 antibody

Three GOLGA8 monoclonal antibodies were produced in rabbits using three different GOLGA8 peptides: (1) GOLGA8N(3–27) EETQ HNKLAAAKKKLKEYWQKNRPR-Cys, (2) GOLGA8N(201-221) CSKAHTEWELEQSLQDQALLK, and (3) GOLGA8N(596–617) DKPTAQPIVQDHQEHPGLGSNC, generated by Pacific Immunology (Ramona, CA). Antibodies were validated for specificity by both immunofluorescence and western blot analysis (Figure S7).

Immunofluorescence

HEK293FT or HeLa cells were grown on glass coverslips in six-well plates. At the endpoint, cells were washed one time with phosphate buffered saline (PBS) and fixed by 4% paraformaldehyde for 30 min at room temperature followed by standard staining protocols using pre-conjugated fluorescent antibodies.

Flow cytometry

A Cy-3-ASO, dextran-Cy3, or transferrin-AF488 was added to cells for the indicated times. Following trypsinization, cells were washed one time with PBS and resuspended in FACS buffer (PBS, 1% BSA, 2 mM EDTA, 50 μg/ml DNaseI) analyzed on a FACS ARIA II. Greater than 10,000 events were collected for each sample and experiments performed in triplicate.

RNA preparation and quantitative real-time PCR

Total RNA was prepared using Zymo (Irvine, CA) Direct-zol RNA miniprep kits according to the manufacturer's instructions. qRT-PCR was performed in triplicate using TaqMan primer probe sets *ARSF*, *CTPS2*, and *LAPTM4B* purchased from Life Technologies (Carlsbad, CA); *GOLGA8* 5′-ACATGGAACGTTCTCTCAGATAC, 5′-GCGCTCTCTAACTCTCCTTTAC, and 5′-TGGCTGTCCGTCT GCAACATTCAT (forward primer, reverse primer, and probe set 1, respectively); 5′-GCAAACAACGAGAGACAGAAAG, 5′-ATGTG GTACAGGTCCGTATTTAG, and 5′-CCGAAAGGGAGCTAGAG GTTCAAATCC (forward primer, reverse primer, probe set 2, respectively); and *MALAT1* 5′-GAATTGCGTCATTTAAAGCCTAGTT, 5′ TCATCCTACCACTCCCAATTAATCT, and 5′-ACGCATTTAC TAAACGCAGACGAAAATGGAX (forward primer, reverse primer, probe, respectively). RNA was normalized to *GAPDH* control using 5′ GAAGGTGAAGGTCGGAGTC (forward), 5′ GAAGATGGTG ATGGGATTTC (reverse), and 5′ CAAGCTTCCCGTTCTCAGCC X (probe). Cycling conditions included reverse transcription step at 50°C for 2 min, 95°C for 2 min and 40× cycling of 95°C for 1 s and 60°C for 20 s using EXPRESS One-Step SuperScript qRT-PCR Universal kit (Thermo Fisher, Waltham, MA).

DGE analysis

Gene expression analysis was performed on total RNA using the QuantSeq 3′ mRNA-Seq Library Prep Kit for Illumina (Lexogen catalog #015). NGS libraries were sequenced on a NovaSeq Instrument (Illumina) to an average depth of 5 million reads and read length of 60 bp. Reads were demultiplexed and aligned to the human reference genome GRCh38 and Ensembl gene models (Homo sapiens, build 96) using the STAR alignment software (version 2.5.1b) with the following run parameters: outFilterMultimapNmax 10, outFilterMatchNmin 23, and seedSearchStartLmax 50. Transcript quantification was performed using Salmon version 0.7.1. Transcript per Million (TPM) was computed for each gene by normalizing gene counts to total mapped reads. Differentially expressed genes were identified by comparing against control sample expression. Gene-specific p values were computed assuming a negative binomial distribution of controls. Genes having a minimum p value less than or equal to 0.05 and fold change greater than 1 were considered differentially expressed.

Statistical analysis

Data are presented as mean ± SE. Statistical analyses were performed using GraphPad Prism 9. An unpaired t test was performed for comparing two experimental groups. p values are indicated using asterisks as follows: ***$p < 0.001$ and ****$p < 0.0001$.

DATA AVAILABILITY

DGE data can be accessed in the GEO database entry GEO: GSE201237.

SUPPLEMENTAL INFORMATION

Supplemental information can be found online at https://doi.org/10.1016/j.omtn.2023.03.017.

ACKNOWLEDGMENTS

We would like to thank Steven Kuntz (Ionis Pharmaceuticals) and Melanie Bell (Ionis Pharmaceuticals) for technical assistance in sequencing library preparation and virus preparation. This work was in part supported by grants from the NIH 5R35GM122476 and 5R01NS027036 to D.W.C., who receives salary support from the Ludwig Institute for Cancer Research. M.W.B. was supported in part by Ruth Kirschstein Institutional National Research Service Award T32 GM008666.

AUTHOR CONTRIBUTIONS

M.A.M., M.R., M.C., and M.W.B. collaborated to perform data acquisition and analysis. S.M., H.-H.B., C.H., and S.D. performed high-throughput data analysis, DGE analysis, and GEO database entry. M.A.M., D.W.C., and C.F.B drafted the manuscript. All authors reviewed and edited the manuscript.

DECLARATION OF INTERESTS

The authors declare no competing interests.

REFERENCES

1. Crooke, S.T., Witztum, J.L., Bennett, C.F., and Baker, B.F. (2018). RNA-targeted therapeutics. Cell Metabol. *27*, 714–739. https://doi.org/10.1016/j.cmet.2018.03.004.

2. Crooke, S.T. (2017). Molecular mechanisms of antisense oligonucleotides. Nucleic Acid Therapeut. *27*, 70–77. https://doi.org/10.1089/nat.2016.0656.

3. Bennett, C.F., Baker, B.F., Pham, N., Swayze, E., and Geary, R.S. (2017). Pharmacology of antisense drugs. Annu. Rev. Pharmacol. Toxicol. *57*, 81–105. https://doi.org/10.1146/annurev-pharmtox-010716-104846.

4. Bennett, C.F., and Swayze, E.E. (2010). RNA targeting therapeutics: molecular mechanisms of antisense oligonucleotides as a therapeutic platform. Annu. Rev. Pharmacol. Toxicol. *50*, 259–293. https://doi.org/10.1146/annurev.pharmtox.010909.105654.

5. Shen, X., and Corey, D.R. (2018). Chemistry, mechanism and clinical status of antisense oligonucleotides and duplex RNAs. Nucleic Acids Res. *46*, 1584–1600. https://doi.org/10.1093/nar/gkx1239.

6. Beltinger, C., Saragovi, H.U., Smith, R.M., LeSauteur, L., Shah, N., DeDionisio, L., Christensen, L., Raible, A., Jarett, L., and Gewirtz, A.M. (1995). Binding, uptake, and intracellular trafficking of phosphorothioate-modified oligodeoxynucleotides. J. Clin. Invest. *95*, 1814–1823. https://doi.org/10.1172/JCI117860.

7. Geary, R.S., Wancewicz, E., Matson, J., Pearce, M., Siwkowski, A., Swayze, E., and Bennett, F. (2009). Effect of dose and plasma concentration on liver uptake and pharmacologic activity of a 2′-methoxyethyl modified chimeric antisense oligonucleotide targeting PTEN. Biochem. Pharmacol. *78*, 284–291. https://doi.org/10.1016/j.bcp.2009.04.013.

8. Liang, X.H., Sun, H., Nichols, J.G., and Crooke, S.T. (2017). RNase H1-dependent antisense oligonucleotides are robustly active in directing RNA cleavage in both the cytoplasm and the nucleus. Mol. Ther. *25*, 2075–2092. https://doi.org/10.1016/j.ymthe.2017.06.002.

9. Juliano, R.L. (2018). Intracellular trafficking and endosomal release of oligonucleotides: what we know and what we don't. Nucleic Acid Therapeut. *28*, 166–177. https://doi.org/10.1089/nat.2018.0727.

10. Koller, E., Vincent, T.M., Chappell, A., De, S., Manoharan, M., and Bennett, C.F. (2011). Mechanisms of single-stranded phosphorothioate modified antisense oligonucleotide accumulation in hepatocytes. Nucleic Acids Res. *39*, 4795–4807. https://doi.org/10.1093/NAR/GKR089.

11. Miller, C.M., Donner, A.J., Blank, E.E., Egger, A.W., Kellar, B.M., Østergaard, M.E., Seth, P.P., and Harris, E.N. (2016). Stabilin-1 and Stabilin-2 are specific receptors for the cellular internalization of phosphorothioate-modified antisense oligonucleotides (ASOs) in the liver. Nucleic Acids Res. *44*, 2782–2794. https://doi.org/10.1093/nar/gkw112.

12. Crooke, S.T., Wang, S., Vickers, T.A., Shen, W., and Liang, X.H. (2017). Cellular uptake and trafficking of antisense oligonucleotides. Nat. Biotechnol. *35*, 230–237. https://doi.org/10.1038/nbt.3779.

13. Prakash, T.P., Graham, M.J., Yu, J., Carty, R., Low, A., Chappell, A., Schmidt, K., Zhao, C., Aghajan, M., Murray, H.F., et al. (2014). Targeted delivery of antisense oligonucleotides to hepatocytes using triantennary N-acetyl galactosamine improves potency 10-fold in mice. Nucleic Acids Res. *42*, 8796–8807. https://doi.org/10.1093/nar/gku531.

14. Juliano, R.L., Carver, K., Cao, C., and Ming, X. (2013). Receptors, endocytosis, and trafficking: the biological basis of targeted delivery of antisense and siRNA oligonucleotides. J. Drug Target. *21*, 27–43. https://doi.org/10.3109/1061186X.2012.740674.

15. Buntz, A., Killian, T., Schmid, D., Seul, H., Brinkmann, U., Ravn, J., Lindholm, M., Knoetgen, H., Haucke, V., and Mundigl, O. (2019). Quantitative fluorescence imaging determines the absolute number of locked nucleic acid oligonucleotides needed for suppression of target gene expression. Nucleic Acids Res. *47*, 953–969. https://doi.org/10.1093/nar/gky1158.

16. Sanjana, N.E., Shalem, O., and Zhang, F. (2014). Improved vectors and genome-wide libraries for CRISPR screening. Nat. Methods *11*, 783–784. https://doi.org/10.1038/nmeth.3047.

17. Wang, T., Wei, J.J., Sabatini, D.M., and Lander, E.S. (2014). Genetic screens in human cells using the CRISPR-Cas9 system. Science *343*, 80–84. https://doi.org/10.1126/science.1246981.

18. Shalem, O., Sanjana, N.E., Hartenian, E., Shi, X., Scott, D.A., Mikkelson, T., Heckl, D., Ebert, B.L., Root, D.E., Doench, J.G., and Zhang, F. (2014). Genome-scale CRISPR-Cas9 knockout screening in human cells. Science *343*, 84–87. https://doi.org/10.1126/science.1247005.

19. Konermann, S., Brigham, M.D., Trevino, A.E., Joung, J., Abudayyeh, O.O., Barcena, C., Hsu, P.D., Habib, N., Gootenberg, J.S., Nishimasu, H., et al. (2015). Genome-scale transcriptional activation by an engineered CRISPR-Cas9 complex. Nature *517*, 583–588. https://doi.org/10.1038/nature14136.

20. Mali, P., Yang, L., Esvelt, K.M., Aach, J., Guell, M., DiCarlo, J.E., Norville, J.E., and Church, G.M. (2013). RNA-guided human genome engineering via Cas9. Science *339*, 823–826. https://doi.org/10.1126/science.1232033.

21. Cong, L., Ran, F.A., Cox, D., Lin, S., Barretto, R., Habib, N., Hsu, P.D., Wu, X., Jiang, W., Marraffini, L.A., and Zhang, F. (2013). Multiplex genome engineering using CRISPR/Cas systems. Science *339*, 819–823. https://doi.org/10.1126/science.1231143.

22. Jinek, M., Chylinski, K., Fonfara, I., Hauer, M., Doudna, J.A., and Charpentier, E. (2012). A programmable dual-RNA-guided DNA endonuclease in adaptive bacterial immunity. Science *337*, 816–821. https://doi.org/10.1126/science.1225829.

23. Xu, X., Hulshoff, M.S., Tan, X., Zeisberg, M., and Zeisberg, E.M. (2020). Crispr/cas derivatives as novel gene modulating tools: possibilities and in vivo applications. Int. J. Mol. Sci. *21*, 3038. https://doi.org/10.3390/ijms21093038.

24. Linnane, E., Davey, P., Zhang, P., Puri, S., Edbrooke, M., Chiarparin, E., Revenko, A.S., Macleod, A.R., Norman, J.C., and Ross, S.J. (2019). Differential uptake, kinetics and mechanisms of intracellular trafficking of next-generation antisense oligonucleotides across human cancer cell lines. Nucleic Acids Res. *47*, 4375–4392. https://doi.org/10.1093/nar/gkz214.

25. Sazani, P., Kang, S.H., Maier, M.A., Wei, C., Dillman, J., Summerton, J., Manoharan, M., and Kole, R. (2001). Nuclear antisense effects of neutral, anionic and cationic oligonucleotide analogs. Nucleic Acids Res. *29*, 3965–3974. https://doi.org/10.1093/NAR/29.19.3965.

26. Concordet, J.P., and Haeussler, M. (2018). CRISPOR: intuitive guide selection for CRISPR/Cas9 genome editing experiments and screens. Nucleic Acids Res. *46*, W242–W245. https://doi.org/10.1093/nar/gky354.

27. Witkos, T.M., and Lowe, M. (2015). The golgin family of coiled-coil tethering proteins. Front. Cell Dev. Biol. *3*, 86. https://doi.org/10.3389/fcell.2015.00086.

28. Nakamura, N., Rabouille, C., Watson, R., Nilsson, T., Hui, N., Slusarewicz, P., Kreis, T.E., and Warren, G. (1995). Characterization of a cis-Golgi matrix protein, GM130. J. Cell Biol. *131*, 1715–1726. https://doi.org/10.1083/jcb.131.6.1715.

29. Lowe, M. (2019). The physiological functions of the Golgin vesicle tethering proteins. Front. Cell Dev. Biol. *7*, 94. https://doi.org/10.3389/fcell.2019.00094.

30. Bekpen, C., and Tautz, D. (2019). Human core duplicon gene families: game changers or game players? Brief. Funct. Genomics *18*, 402–411. https://doi.org/10.1093/bfgp/elz016.

31. Wang, S., Sun, H., Tanowitz, M., Liang, X.H., and Crooke, S.T. (2016). Annexin A2 facilitates endocytic trafficking of antisense oligonucleotides. Nucleic Acids Res. *44*, 7314–7330. https://doi.org/10.1093/NAR/GKW595.

32. Juliano, R.L., and Carver, K. (2015). Cellular uptake and intracellular trafficking of oligonucleotides. Adv. Drug Deliv. Rev. *87*, 35–45. https://doi.org/10.1016/J.ADDR.2015.04.005.

33. Liang, X.H., Sun, H., Hsu, C.-W., Nichols, J.G., Vickers, T.A., De Hoyos, C.L., and Crooke, S.T. (2020). Golgi-endosome transport mediated by M6PR facilitates release of antisense oligonucleotides from endosomes. Nucleic Acids Res. *48*, 1372–1391. https://doi.org/10.1093/NAR/GKZ1171.

34. Bonifacino, J.S., and Rojas, R. (2006). Retrograde transport from endosomes to the trans-Golgi network. Nat. Rev. Mol. Cell Biol. *7*, 568–579. https://doi.org/10.1038/nrm1985.

35. Hayes, G.L., Brown, F.C., Haas, A.K., Nottingham, R.M., Barr, F.A., and Pfeffer, S.R. (2009). Multiple rab GTPase binding sites in GCC185 suggest a model for vesicle tethering at the trans-golgi. Mol. Biol. Cell *20*, 209–217. https://doi.org/10.1091/MBC.E08-07-0740.

36. Reddy, J.v., Burguete, A.S., Sridevi, K., Ganley, I.G., Nottingham, R.M., and Pfeffer, S.R. (2006). A functional role for the GCC185 Golgin in mannose 6-phosphate receptor recycling. Mol. Biol. Cell *17*, 4353–4363. https://doi.org/10.1091/MBC.E06-02-0153/ASSET/IMAGES/LARGE/ZMK0100678100010.JPEG.

37. Joung, J., Konermann, S., Gootenberg, J.S., Abudayyeh, O.O., Platt, R.J., Brigham, M.D., Sanjana, N.E., and Zhang, F. (2017). Genome-scale CRISPR-Cas9 knockout and transcriptional activation screening. Nat. Protoc. *12*, 828–863. https://doi.org/10.1038/nprot.2017.016.